3D STEGANALYSIS USING THE EXTENDED LOCAL FEATURE SET

Zhenyu Li[⋆] *Daofu Gong*[†] *Fenlin Liu*[†] *Adrian G. Bors*[⋆]

[⋆] Department of Computer Science, University of York, York YO10 5GH, UK
[†] Zhengzhou Institute of Information Science and Technology, Zhengzhou 450000, China

ABSTRACT

3D steganalysis aims to find the changes embedded through steganographic or information hiding algorithms into 3D models. This research study proposes to use new 3D features, such as the edge vectors, represented in both Cartesian and Laplacian coordinate systems, together with other steganalytic features, for improving the results of 3D steganalysers. In this way the local feature vector used by the steganalyzer is extended to 124 dimensions. We test the performance of the extended local feature set, and compare it to four other steganalytic features, when detecting the stego-objects watermarked by six information hiding algorithms.

Index Terms— 3D steganalysis, local features, information hiding

1. INTRODUCTION

3D objects are becoming increasingly used in many application areas, such as computer aided design, 3D printing, virtual reality, augmented reality, medical imaging and so on. A number of watermarking and steganographic methods have been proposed for embedding information into the 3D objects for various applications [1, 2, 3, 4, 5, 6]. The embedding changes produced to the 3D objects are supposed not to be noticeable by the naked eye. Steganalysis is the technique that can identify whether any information was embedded in the given object or not. Many steganalytic methods have been proposed for audio signals [7, 8], digital images [9, 10, 11, 12] or video signals [13, 14].

While 3D objects can be represented in various ways, their most usual data representation is by means of meshes. Such irregular representations, modelling complex 3D objects, are very different from the regular structural arrays representing digital images or video signals. Consequently, the existing image and video steganalytic algorithms cannot be successfully applied to 3D objects. The first steganalytic algorithm for 3D meshes was proposed in [15]. This 3D steganalytic algorithm is based on the 208-dimensional feature set of 3D meshes, called YANG208, and using quadratic discriminate analysis, for distinguishing stego-objects from cover-objects. More recently, Yang *et al.* [16, 4] proposed a new steganalytic algorithm, specifically designed for the robust 3D watermarking algorithm, MRS, proposed in [1]. The limitation of this algorithm is that it is only effective for the information embedded by the MRS algorithm and would not be useful when the mesh is embedded by other information hiding algorithms. Li and Bors proposed the 52-dimensional Local Feature Set (LFS52) in [17], which simplified the 208-dimensional feature set YANG208 proposed in [15] and included some new geometric feature for steganalysis, such as the vertex normal, the curvature ratio and the Gaussian curvature. In addition to LFS52, other geometric features extracted from the mesh, represented in the spherical coordinate system, form the 76-dimensional feature set for 3D steganalysis in [18]. Meanwhile, Kim *et al.* [19] extended the approach from [17], and proposed to use some additional features such as the edge normal, the mean curvature and the total curvature in addition to LFS52, forming the LFS64 feature set for 3D steganalysis. Li and Bors [20] proposed a feature selection algorithm based on the features' relevance and robustness, in order to address the cover source mismatch problem in 3D steganalysis.

Nevertheless, the steganalysis results for 3D wavelet-based watermarking algorithms require further improvement, according to the experimental results reported in [18]. In this paper, we propose to use some new features derived from the edge vectors of the mesh objects for 3D steganalysis. Then, we combine the newly proposed features with the LFS76 feature set, which is then compared against other four steganalytic feature sets, when detecting the stego-objects embedded by six information hiding algorithms. In Section 2 we describe the existing local feature set used for 3D steganalysis, while in Section 3 we describe the new features that we propose to add for improving the results of 3D steganalysis. In Section 4 we present the experimental results, while in Section 5 we draw the conclusions of this study.

2. LOCAL FEATURE SET FOR 3D STEGANALYSIS

In this section, we provide a brief introduction of the 3D steganalytic approach based on the local feature set, LFS76, proposed in [18]. The 3D steganalyzer is trained through the following processing stages: preprocessing, feature extraction and supervised learning. During the preprocessing step, a smoothed version of the given original mesh, $\mathcal{O}'$, is obtained

by applying one iteration of Laplacian smoothing on the original mesh, $\mathcal{O}$. Then, the original mesh and its smoothed version are both normalized by using rotation and scaling.

19 geometric features, characterizing the local geometry of 3D shapes, are extracted from the original mesh, $\mathcal{O}$, and its smoothed version, $\mathcal{O}'$ in order to be used as inputs to the steganalyzer in [18]. These geometric features define the vertex coordinates and norms in the Cartesian and Laplacian coordinate systems, the face normal, the dihedral angle, the vertex normal, the Gaussian curvature, the curvature ratio, the vertex coordinates and edge length in the spherical coordinate system. The differences between the mentioned geometric features from $\mathcal{O}$ and those from $\mathcal{O}'$ are denoted as vector $\mathbf{\Phi} = \{\phi_t | t = 1, 2, .., 19\}$. Afterwards, the first four statistical moments, representing the mean, variance, skewness and kurtosis, of the logarithm of the differences, $\{\lg(\phi_t) | \phi_t \in \mathbf{\Phi}\}$, are considered as the steganalytic features, resulting in the 76-dimensional local feature set, LFS76.

The steganalyzers are trained using the Fisher Linear Discriminant (FLD) ensemble which is broadly used for image steganalysis as well [9, 10, 11]. The FLD ensemble includes a number of base learners trained uniformly on the randomly selected feature subsets extracted from the whole training data. The FLD ensemble uses the majority voting to combine the results of all base learners, but achieves much higher accuracy than any individual base learner [21, 22].

3. EXTENDED LOCAL FEATURE SET

In the following we consider a set of new 3D features, in order to be added to those that have been already used in [15, 18], in order to improve the performance of 3D steganalyzers. We propose to use the edge vectors in both the Cartesian and the Laplacian coordinate systems to extract steganalytic features. Let us assume that we have a given mesh $\mathcal{O} = \{V, F, E\}$, containing the vertex set $V = \{v(i) | i = 1, 2, \ldots, |V|\}$, where $|V|$ represents the number of vertices in the object $\mathcal{O}$, its face set F, and its edge set E, respectively. We define the 1-ring neighbourhood $\mathcal{N}(v(i))$ of a vertex $v(i)$ as $\{v(j) \in \mathcal{N}(v(i)) | e(i,j) \in E\}$, where $e(i,j)$ is the edge connecting vertices $v(i)$ and $v(j)$.

When extracting the steganalytic features, we first apply one iteration of Laplacian smoothing to the original object. Then, the difference between the edge vector in the Cartesian coordinate system from the original mesh, $\mathbf{e}_c(i,j)$, and that from the smoothed mesh, $\mathbf{e}'_c(i,j)$ are calculated in four different ways. Firstly, the absolute differences are calculated for the x, y, z-components of the vector in the Cartesian coordinate system, such as:

$$\begin{aligned} \phi_{20}(i,j) &= |\mathbf{e}_{c,x}(i,j) - \mathbf{e}'_{c,x}(i,j)|, \\ \phi_{21}(i,j) &= |\mathbf{e}_{c,y}(i,j) - \mathbf{e}'_{c,y}(i,j)|, \\ \phi_{22}(i,j) &= |\mathbf{e}_{c,z}(i,j) - \mathbf{e}'_{c,z}(i,j)|, \end{aligned} \tag{1}$$

where $\mathbf{e}_{c,x}(i,j)$ represents the x-component of the vector $\mathbf{e}_c(i,j)$ in the Cartesian coordinate system, defined as

$$\mathbf{e}_{c,x}(i,j) = v_{c,x}(j) - v_{c,x}(i), \tag{2}$$

where $v_{c,x}(i)$ represent the x-coordinate of the ith vertex in the mesh represented in the Cartesian coordinate system.

Secondly, the norm of the difference between the vectors, $\mathbf{e}_c(i,j)$ and $\mathbf{e}'_c(i,j)$, is calculated as

$$\phi_{23}(i,j) = \|\mathbf{e}_c(i,j) - \mathbf{e}'_c(i,j)\|, \tag{3}$$

and the actual feature is made up of the absolute differences between the norms of the two vectors, namely,

$$\phi_{24}(i,j) = |\,\|\mathbf{e}_c(i,j)\| - \|\mathbf{e}'_c(i,j)\|\,|. \tag{4}$$

Moreover, the angle between the two edge vectors, $\mathbf{e}_c(i,j)$ and $\mathbf{e}'_c(i,j)$, is considered as a feature as well,

$$\phi_{25}(i,j) = \arccos \frac{\mathbf{e}_c(i,j) \cdot \mathbf{e}'_c(i,j)}{\|\mathbf{e}_c(i,j)\| \cdot \|\mathbf{e}'_c(i,j)\|}. \tag{5}$$

In the following, we consider the edge vectors in the Laplacian coordinate system as the geometric features. The Laplacian coordinates of the ith vertex, $[v_{l,x}(i), v_{l,y}(i), v_{l,z}(i)]$, are the ith row of matrix $\mathbf{L}$, given by

$$\mathbf{L} = \mathbf{M} \begin{bmatrix} v_{c,x}(1) & v_{c,y}(1) & v_{c,z}(1) \\ v_{c,x}(2) & v_{c,y}(2) & v_{c,z}(2) \\ \cdots & \cdots & \cdots \\ v_{c,x}(|V|) & v_{c,y}(|V|) & v_{c,z}(|V|) \end{bmatrix} \tag{6}$$

where $v_{c,x}(i)$ is the x-coordinate of the ith vertex in the Cartesian coordinate system, $\mathbf{M}$ is the *Kirchhoff* matrix [23]

$$\mathbf{M}_{i,j} = \begin{cases} |\mathcal{N}(v(i))| & \text{if} \quad i = j \\ -1 & \text{if} \quad i \neq j \\ 0 & \text{otherwise} \end{cases} \qquad 1 \leq i, j \leq |V| \tag{7}$$

The x-component of the edge vector $\mathbf{e}_l(i,j)$ in the Laplacian coordinate system is defined as

$$\mathbf{e}_{l,x}(i,j) = v_{l,x}(j) - v_{l,x}(i), \tag{8}$$

where $v_{l,x}(i)$ is the x-coordinate of the ith vertex in the mesh represented in the Laplacian coordinate system.

Various features, $\{\phi_t(i,j) | t = 26, ..., 31\}$, in order to model the differences between the edge vectors in the Laplacian coordinate system form the original mesh and those from the smoothed mesh, are calculated in a similar way as for the Cartesian coordinate calculations from equations (1), (3), (4) and (5).

Eventually, we combine the 19 features proposed for 3D steganalysis in [18] and the 12 new ones proposed in this study into the set, $\mathbf{\Phi} = \{\phi_t | t = 1, 2, .., 31\}$. Then, we follow the same approach as in [18] to form the steganalytic features. Considering the first four statistical moments, representing the mean, variance, skewness and kurtosis, of the logarithm of the statistics, $\{\lg(\phi_t) | \phi_t \in \mathbf{\Phi}\}$, we have the 124-dimensional Extended Local Feature Set, denoted as ELFS124.

4. EXPERIMENTAL RESULTS

In the following we provide the results for the proposed 3D steganalytic approach on 354 cover 3D objects from the Princeton Mesh Segmentation project database [24]. This database contains a large variety of shapes, representing the human body under a variety of postures, statues, animals, toys, tools and so on.

In the following we consider identifying the 3D stego-meshes produced by using six different embedding algorithms: the 3D Wavelet-based High Capacity (WHC) watermarking method and 3D Wavelet-based FRagile (WFR) watermarking method proposed in [2]; the Multi-Layer Steganography (MLS) provided in [3]; two blind robust watermarking algorithms based on modifying the Mean or the Variance of the distribution of the vertices' Radial distances in the Spherical coordinate system, denoted as MRS and VRS, from [1] and the Steganalysis-Resistant Watermarking (SRW) method proposed in [4]. In the case of WHC algorithm from [2], the value of the controlling parameter is considered as $\epsilon_{hc} = 100$. Meanwhile, for the WFR algorithm, we consider the parameter $\Delta_\theta = \pi/3$ while the other parameters are identical to the values given in [2]. When using MLS method from [3], we set the number of layers to 10, and consider the number of intervals as 10000. For MRS and VRS watermarking methods from [1], we consider $\alpha = 0.04$ for the watermark strength, while fixing the incremental step size to $\Delta k = 0.001$ and the message payload as 64 bits. During the generation of the stego-meshes using the SRW method from [4], we set the parameter $K = 128$ which determines the number of bins in the histogram of the radial distance coordinates for all vertices. According to [4], the upper bound of the embedding capacity is $\lfloor (K-2)/2 \rfloor$ bits. The parameter that controls the watermarking robustness of SRW is n_{thr}, which is set at 20. If the smallest number of elements in the bins from the objects is less than 20, we would choose the smallest nonzero number of elements in the bins as n_{thr}. The embedded information is a pseudorandom bit stream which simulates the secret messages or watermarks hidden by the steganographier.

The proposed feature set, ELFS124, is extracted from the cover-meshes and the corresponding stego-meshes when embedded with information by various 3D embedding algorithms. During the preprocessing stage, we firstly apply one iteration of Laplacian smoothing on both cover-meshes and stego-meshes, by setting the scale factor as $\lambda = 0.2$. The 3D steganalytic features are extracted as described in Sections 2 and 3. We consider the proposed feature set ELFS124, and compare its results against other 3D steganalytic feature sets such as, YANG208 [15], LFS52 [17], LFS64 [19] and LFS76 [18]. The steganalyzers are trained using the FLD ensemble as in [18]. For each steganalyzer, we split the 354 pairs of cover-mesh and stego-mesh into 260 pairs for training and 94 pairs for testing, repeating the experiments independently for 30 times. The steganalysis results are assessed by calculating the areas under the Receiver Operating Characteristic (ROC) curves of the testing results for all 30 trials. The ROC curve is created by plotting the true positive rate against the false positive rate at various threshold settings. The larger area under the ROC curve represents higher accuracy of the testing results. The ROC curves for the 3D steganalysis results when the information was embedded by WHC or WFR for one trial, using the FLD ensembles trained on various 3D steganalytic feature sets, are provided in Figure 1. It can be observed from Figure 1 that the proposed feature set, ELFS124, achieves the best performance among the 3D steganalytic feature sets being tested.

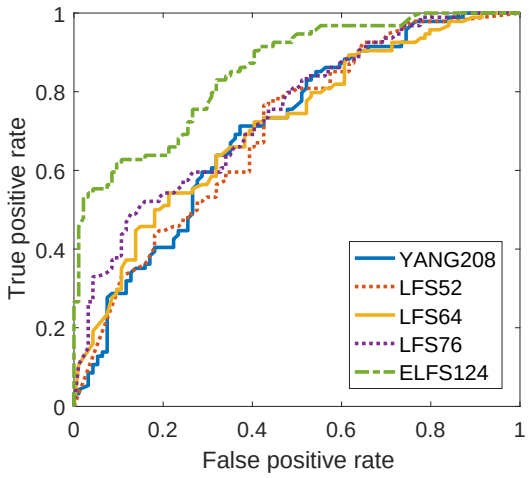

(a) WHC [2]

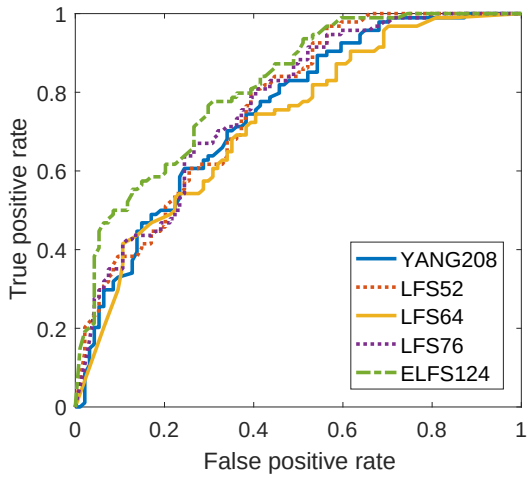

(b) WFR [2]

Fig. 1. ROC curves for the detection results for the steganalyzers trained by five feature sets when testing for the WHC and WFR algorithms, respectively.

The confidence intervals of the areas under the ROC curves of the steganalysis results for six information hiding

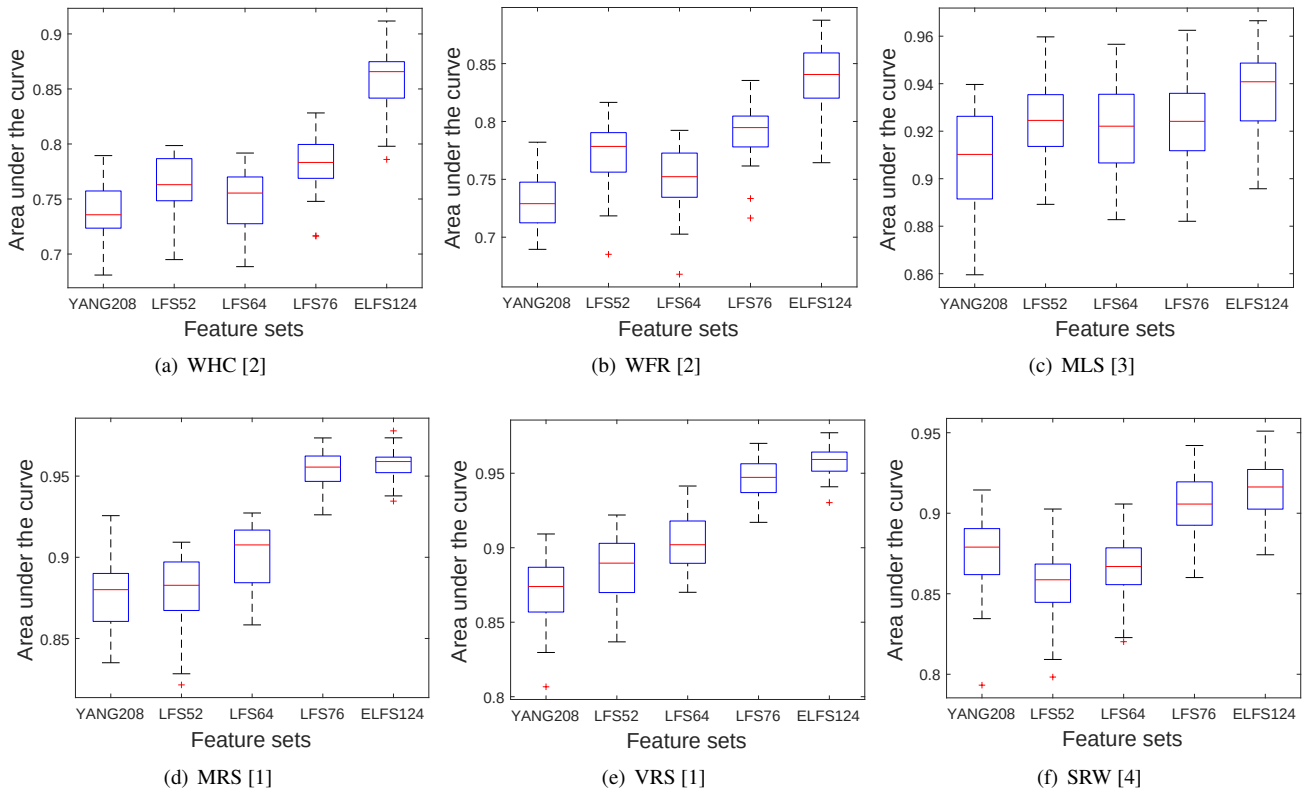

(a) WHC [2] (b) WFR [2] (c) MLS [3]

(d) MRS [1] (e) VRS [1] (f) SRW [4]

Fig. 2. Box plots showing the confidence intervals for the area under the ROC curves of the detection results for the trained steganalyzers when testing over 30 independent splits for the six 3D information embedding algorithms.

algorithms when testing over 30 splits of training/testing data are shown as box plots in Figure 2. The proposed feature set, ELFS124, shows better performance when compared to the other four steganalytic feature sets. It can be observed from Figures 2(a) and 2(b) that the advantage of ELFS124 over the other feature sets is quite obvious when detecting the stego-objects embedded by the two 3D wavelet-based watermarking algorithms, WHC and WFR. It is interesting that the LFS52 feature set achieves better steganalysis performance than LFS64 in the context of WHC, WFR and MLS, as shown in Figures 2(a)-(c). We deduce that this is because the features introduced in LFS64 are more efficient when the embedding changes are more significant.

5. CONCLUSION

The contribution of the paper consists in proposing a new set of local features for 3D steganalysis. We consider the edge vectors of the mesh, represented in both the Cartesian and the Laplacian coordinate systems, which are extracted from the geometric features of the original mesh and its smoothed version. Then, an extended local feature set is obtained by combining the newly proposed features with the existing feature set, LFS76, from [18]. According to the experimental results, the extended local feature set shows better performance than LFS76 and other existing 3D steganalytic features, when identifying the stego-objects watermarked by several 3D information hiding algorithms. 3D steganalysis and 3D watermarking have many potential applications, such as copyright protection and covertly storing relevant information, not only to be used in virtual graphics and vision but which also can be embedded into real 3D objects through 3D printing.

6. REFERENCES

[1] Jae-Won Cho, Rémy Prost, and Ho-Youl Jung, "An oblivious watermarking for 3-D polygonal meshes using distribution of vertex norms," *IEEE Transactions on Signal Processing*, vol. 55, no. 1, pp. 142–155, 2007.

[2] Kai Wang, Guillaume Lavoué, Florence Denis, and Atilla Baskurt, "Hierarchical watermarking of semiregular meshes based on wavelet transform," *IEEE Transactions on Information Forensics and Security*, vol. 3, no. 4, pp. 620–634, 2008.

[3] Min-Wen Chao, Chao-hung Lin, Cheng-Wei Yu, and Tong-Yee Lee, "A high capacity 3D steganography al-

gorithm," *IEEE Transactions on Visualization and Computer Graphics*, vol. 15, no. 2, pp. 274–284, 2009.

[4] Ying Yang, Ruggero Pintus, Holly Rushmeier, and Ioannis Ivrissimtzis, "A 3D steganalytic algorithm and steganalysis-resistant watermarking," *IEEE Transactions on Visualization and Computer Graphics*, vol. 23, no. 2, pp. 1002–1013, Feb 2017.

[5] Vincent Itier and William Puech, "High capacity data hiding for 3D point clouds based on static arithmetic coding," *Multimedia Tools and Applications*, vol. 76, no. 24, pp. 26421–26445, 2017.

[6] Zhenyu Li, Sébastien Beugnon, William Puech, and Adrian G. Bors, "Rethinking the high capacity 3D steganography: Increasing its resistance to steganalysis," in *Proc. IEEE Int. Conf. on Image Processing*, 2017, pp. 510–514.

[7] Y. Ren, T. Cai, M. Tang, and L. Wang, "AMR steganalysis based on the probability of same pulse position," *IEEE Transactions on Information Forensics and Security*, vol. 10, no. 9, pp. 1801–1811, 2015.

[8] Yanzhen Ren, Jing Yang, Jinwei Wang, and Lina Wang, "AMR steganalysis based on second-order difference of pitch delay," *IEEE Transactions on Information Forensics and Security*, vol. 12, no. 6, pp. 1345–1357, 2017.

[9] Zhenyu Li, Zongyun Hu, Xiangyang Luo, and Bin Lu, "Embedding change rate estimation based on ensemble learning," in *Proc. ACM Workshop on Information Hiding and Multimedia Security*, 2013, pp. 77–84.

[10] Xiaofeng Song, Fenlin Liu, Chunfang Yang, Xiangyang Luo, and Yi Zhang, "Steganalysis of adaptive JPEG steganography using 2D gabor filters," in *Proc. ACM Workshop on Information Hiding and Multimedia Security*, 2015, pp. 15–23.

[11] Weixuan Tang, Haodong Li, Weiqi Luo, and Jiwu Huang, "Adaptive steganalysis based on embedding probabilities of pixels," *IEEE Transactions on Information Forensics and Security*, vol. 11, no. 4, pp. 734–745, 2016.

[12] Jian Ye, Jiangqun Ni, and Yang Yi, "Deep learning hierarchical representations for image steganalysis," *IEEE Transactions on Information Forensics and Security*, vol. 12, no. 11, pp. 2545–2557, 2017.

[13] Keren Wang, Hong Zhao, and Hongxia Wang, "Video steganalysis against motion vector-based steganography by adding or subtracting one motion vector value," *IEEE Transactions on Information Forensics and Security*, vol. 9, no. 5, pp. 741–751, 2014.

[14] Hong Zhang, Yun Cao, and Xianfeng Zhao, "A steganalytic approach to detect motion vector modification using near-perfect estimation for local optimality," *IEEE Transactions on Information Forensics and Security*, vol. 12, no. 2, pp. 465–478, 2017.

[15] Ying Yang and Ioannis Ivrissimtzis, "Mesh discriminative features for 3D steganalysis," *ACM Transactions on Multimedia Computing, Communications, and Applications*, vol. 10, no. 3, pp. 27:1–27:13, 2014.

[16] Ying Yang, Ruggero Pintus, Holly Rushmeier, and Ioannis Ivrissimtzis, "A steganalytic algorithm for 3D polygonal meshes," in *Proc. IEEE Int. Conf. on Image Processing*, 2014, pp. 4782–4786.

[17] Zhenyu Li and Adrian G. Bors, "3D mesh steganalysis using local shape features," in *Proc. IEEE Int. Conf. on Acoustics, Speech and Signal Processing*, 2016, pp. 2144–2148.

[18] Zhenyu Li and Adrian G. Bors, "Steganalysis of 3D objects using statistics of local feature sets," *Information Sciences*, vol. 415-416, pp. 85–99, 2017.

[19] Dongkyu Kim, Han-Ul Jang, Hak-Yeol Choi, Jeongho Son, In-Jae Yu, and Heung-Kyu Lee, "Improved 3D mesh steganalysis using homogeneous kernel map," in *Proc. Int. Conf. on Information Science and Applications*, 2017, pp. 358–365.

[20] Zhenyu Li and Adrian G. Bors, "Selection of robust features for the cover source mismatch problem in 3D steganalysis," in *Proc. Int. Conf. on Pattern Recognition*, 2016, pp. 4256–4261.

[21] Jan Kodovskỳ, Jessica Fridrich, and Vojtěch Holub, "Ensemble classifiers for steganalysis of digital media," *IEEE Transactions on Information Forensics and Security*, vol. 7, no. 2, pp. 432–444, 2012.

[22] Remi Cogranne and Jessica Fridrich, "Modeling and extending the ensemble classifier for steganalysis of digital images using hypothesis testing theory," *IEEE Transactions on Information Forensics and Security*, vol. 10, no. 12, pp. 2627–2642, 2015.

[23] Béla Bollobás, *Modern graph theory*, vol. 184, Springer Science & Business Media, 2013.

[24] Xiaobai Chen, Aleksey Golovinskiy, and Thomas Funkhouser, "A benchmark for 3D mesh segmentation," *ACM Transactions on Graphics*, vol. 28, no. 3, pp. 73:1–73:12, 2009.